DOI: 10.26599/FSHW.2026.9251240

Contents lists available at SciOpen

Food Science and Human Wellness

journal homepage: https://www.sciopen.com/journal/2097-0765

China Food Publishing Co.

From DNA Aptamer Selection to Label-Free Fluorescent Biosensor for Chebulinic Acid

Keren Chen[a], Zimian Ding[b], Yangzi Zhang[a], Lingyun Wang[a], Qingfang Zheng[a], Longjiao Zhu[a], Wentao Xu[a*]

[a] *Food Laboratory of Zhongyuan, Key Laboratory of Precision Nutrition and Food Quality, Department of Nutrition and Health, China Agricultural University, Beijing, 100193, China*

[b] *Institute of Medicinal Plant Development, Chinese Academy of Medical Sciences & Peking Union Medical College, Beijing 100193, China*

ABSTRACT: Chebulinic acid is a bioactive hydrolyzable tannin of increasing interest in natural product research, quality control, and pharmaceutical studies. In this work, four candidate DNA aptamers were identified using a restriction endonuclease-assisted SELEX (REase-SELEX) strategy, and Aptamer 1 was selected based on its enrichment level, predicted structural stability, thermal stability, and structural characteristics. A label-free fluorescent aptasensor was developed using thioflavin T (ThT) as the signal reporter. Structural prediction indicated that the selected aptamer was a G-rich sequence containing multiple stem-loop motifs and potential G-quadruplex-forming regions. Molecular docking further suggested possible binding modes between the aptamer and chebulinic acid involving multiple noncovalent interactions. The binding affinity was further validated by microscale thermophoresis and a gold nanoparticle-based colorimetric assay, yielding dissociation constants of 4.112 and 2.770 μM, respectively. Under optimized conditions, the proposed aptasensor exhibited a good linear response toward chebulinic acid in the range of 0.1-50 μM, with a regression equation of Y = -1.260X + 248.6 and an R^2 of 0.9872. The limit of detection (LOD) was 8.29 nM. In addition, the sensor showed good selectivity and satisfactory recovery in a compound blank matrix and 10% fetal bovine serum (FBS), with recoveries of 94.3%-102.9%. These results demonstrate that the proposed platform provides a simple, low-cost, and sensitive strategy for chebulinic acid detection.

Keywords: Chebulinic acid; DNA aptamers; REase-SELEX; Label-free biosensing; Thioflavin T

1. Introduction

Chebulinic acid is a bioactive hydrolyzable tannin widely found in medicinal plants and plant-derived products. It has attracted increasing attention because of its diverse biological activities, including anti-inflammatory, antioxidant, antimicrobial, and antitumor effects [1]. Owing to its pharmacological relevance and functional potential, reliable analysis of chebulinic acid is increasingly needed. This demand is particularly important for natural product and traditional Chinese medicine quality control, formulation development, pharmacokinetic studies, and stability evaluation [2,3]. Therefore, establishing reliable and convenient analytical methods for chebulinic acid is of considerable significance.

***Corresponding author**
xuwentao@cau.edu.cn (W. Xu)

Received 5 June 2026
Received in revised from 23 June 2026
Accepted 5 August 2026

At present, chebulinic acid is mainly determined by chromatographic and mass spectrometric methods, such as HPLC- and LC-MS-based assays [4,5]. Although these approaches provide high sensitivity and accuracy, they often require expensive instrumentation, laborious sample pretreatment, and trained operators, which may limit their practicality for rapid or routine analysis [6]. Accordingly, alternative sensing strategies that are simple, rapid, cost-effective, and sensitive remain highly desirable.

Aptamers are single-stranded nucleic acids obtained by systematic evolution of ligands by exponential enrichment (SELEX) and are capable of binding their targets with high affinity and specificity [7]. Because of their facile synthesis, good stability, and versatile recognition capability, aptamers have become attractive recognition elements for biosensors [6]. In recent years, aptamer-based biosensors have shown great promise for the detection of various analytes. However, many reported aptasensors rely on covalent labeling with signal molecules, which may increase assay cost and disturb the native folding behavior of aptamers [8,9]. Therefore, the development of label-free aptasensing strategies is of particular interest.

Thioflavin T (ThT) is a small-molecule fluorescent dye that can bind to specific nucleic acid structures, including G-quadruplexes, hairpin-like structures, and duplex motifs, resulting in enhanced fluorescence [6,10]. Therefore, ThT was selected as a label-free signal reporter in this study because the G-rich chebulinic acid aptamer was predicted to contain folded structural motifs that may provide ThT-binding sites.

In the present work, as shown in Figure 1, a chebulinic acid-specific DNA aptamer was screened by the REase-SELEX strategy, and a label-free fluorescent aptasensor was subsequently developed using ThT as the signal reporter. The structural characteristics, binding behavior, sensing performance, and applicability in complex matrices were systematically investigated. This study provides a new aptamer recognition element and a simple, low-cost, and sensitive platform for chebulinic acid detection.

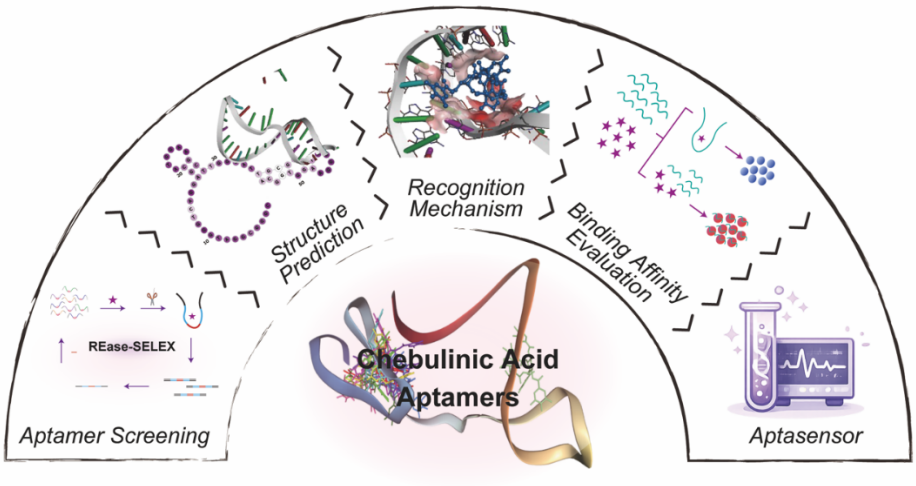

Figure 1. Schematic workflow of REase-SELEX-based screening, structural characterization, binding affinity evaluation, and label-free fluorescent biosensing application of chebulinic acid-specific DNA aptamers.

2. Materials and methods

2.1 Materials

All oligonucleotides used in this study were custom synthesized by Sangon Biotech Co., Ltd. (Shanghai, China). Chebulinic acid was purchased from Nature Standard Co., Ltd. (Shanghai, China). Tris(hydroxymethyl)aminomethane (Tris)

was obtained from Biotopped Technologies Co., Ltd. (Beijing, China). Sodium chloride (NaCl), potassium chloride (KCl), thioflavin T (ThT), glucose, ascorbic acid, gallic acid, and tannic acid were purchased from Sigma-Aldrich Chemical Co., Ltd. (St. Louis, MO, USA). Magnesium chloride hexahydrate ($MgCl_2 \cdot 6H_2O$) was supplied by Sinopharm Chemical Reagent Co., Ltd. (Shanghai, China). Fetal bovine serum (FBS) was obtained from ExCell Bio Co., Ltd. (Suzhou, China). PCR-related reagents were purchased from Sangon Biotech Co., Ltd. (Shanghai, China). Lambda exonuclease was obtained from New England Biolabs (NEB, Ipswich, MA, USA), and HindIII was purchased from Takara Bio Inc. (Shiga, Japan). SYBR Green I was obtained from Solarbio Science & Technology Co., Ltd. (Beijing, China).

2.2 Aptamer selection

Chebulinic acid-specific aptamers were screened using the restriction endonuclease-assisted SELEX (REase-SELEX) method. Briefly, the random ssDNA library was first mixed with a fixed complementary sequence and annealed in a PCR thermocycler by gradually cooling from 95°C to 25°C to form duplex complexes. Chebulinic acid was then added and incubated with the duplex library, allowing those ssDNA sequences capable of specifically binding the target to dissociate from the duplex and form ssDNA-target complexes. Subsequently, a restriction endonuclease was introduced to digest the remaining undissociated duplex complexes, thereby eliminating their ability to serve as templates for subsequent amplification, while the target-bound ssDNA sequences were retained.

The retained sequences were amplified by PCR using a 5′-phosphorylated reverse primer. The PCR products were treated with Lambda exonuclease, which selectively digested the 5′-phosphorylated strand of the double-stranded DNA products, leaving the complementary non-phosphorylated strand as ssDNA. The resulting ssDNA was purified and used as the secondary library for the next round of selection. By repeating the steps of annealing, target incubation, restriction enzyme digestion, PCR amplification, and ssDNA preparation over multiple rounds, sequences with high affinity and specificity toward chebulinic acid were progressively enriched. After completion of the selection process, the final enriched library was subjected to high-throughput sequencing to obtain candidate chebulinic acid aptamer sequences.

2.3 Prediction of aptamer structure

The secondary structures of the candidate chebulinic acid aptamers were predicted using the RNAfold web server [11], with DNA folding parameters selected. Structural images were generated using the “MFE structure drawing encoding base-pair probabilities” mode, and the predicted secondary structures were further visualized using FORNA.

2.4 Melting temperature (Tm) measurement

Melting experiments were performed using a Cary Eclipse fluorescence spectrophotometer equipped with a thermoelectrically controlled cell holder. The annealed sequence was introduced into the buffer solution. Changes in SYBR Green I fluorescence were monitored across a temperature range of 25-95℃, with a heating rate of 0.2℃/min.

2.5 Circular dichroism (CD) experiments

The CD spectra of 5 μM aptamers in the buffer solution were recorded using a JASCO J-1500 spectropolarimeter (Tokyo, Japan) at 20℃. Three scans were performed over the wavelength range of 200-340 nm at a scanning rate of 1 nm/s. The buffer solution background was subtracted from the CD data.

2.6 Microscale thermophoresis (MST)

MST binding experiments were performed with a fixed concentration of fluorophore-labeled aptamer and varying concentrations of chebulinic acid. The experiments were conducted using a Monolith NT.115 Pico instrument (NanoTemper Technologies, Munich, Germany) at 25℃, with 20% MST power and 20% LED intensity, using standard capillaries. Each experiment was repeated three times.

2.7 Molecular docking

The secondary structures of the candidate DNA aptamers were first predicted using the RNAfold web server [11]. Based on these predictions, the corresponding 3D aptamer structures were generated using RNAComposer [12]. The resulting RNA 3D structures were manually converted into DNA 3D structures and subsequently energy-minimized in BIOVIA Discovery Studio Visualizer to obtain energetically favorable DNA conformations. The chemical structure of chebulinic acid was retrieved from PubChem, and its geometry was further optimized using ChemOffice. Molecular docking between chebulinic acid and the aptamers was then performed using the HDOCK web server [13], with chebulinic acid treated as the ligand and the aptamers as the receptors. The resulting aptamer-ligand interaction models were analyzed using BIOVIA Discovery Studio Visualizer.

2.8 Gold nanoparticle (AuNP) colorimetric assays

AuNP-based colorimetric assays were performed to evaluate the interaction between chebulinic acid and the DNA aptamer based on the salt-induced aggregation behavior of citrate-capped AuNPs [14-17]. Briefly, 5 μL of aptamer solution (1 μM) was mixed with 5 μL of chebulinic acid at different concentrations and incubated for 40 min. Then, 100 μL of citrate-capped AuNPs was added, followed by another 40 min incubation. Subsequently, 8 μL of NaCl solution (0.5 M) was added, and the mixture was incubated for a final 15 min. The color change of the solution was photographed, and the absorbance values at 525 nm and 626 nm were recorded using a microplate reader. The absorbance ratio A626/A525 was used to evaluate the binding affinity of the chebulinic acid aptamer. In the dispersed state of AuNPs, the absorbance at 525 nm was high and that at 626 nm was low, resulting in a low A626/A525 value. The apparent dissociation constant was obtained by fitting the concentration-dependent response using a one-site saturation binding model: $Y = Bmax \cdot X/(Kd + X)$, where Y represents the A626/A525 response, X represents the chebulinic acid concentration, Bmax represents the maximum response, and Kd represents the apparent dissociation constant.

2.9 Evaluation of biosensing performance

Sensitivity test. The sensitivity of the aptasensor was evaluated by detecting chebulinic acid at known concentrations and constructing a calibration curve based on changes in the fluorescence intensity of ThT. Different concentrations of chebulinic acid and ThT (final concentration: 2.5 μM) were simultaneously added

to a buffer solution containing 1 μM aptamer (10 mM Tris-HCl, 10 mM $MgCl_2$, 20 mM KCl, 1 mM DTT, pH 7.4), yielding final chebulinic acid concentrations of 0, 0.1, 0.2, 0.5, 1, 2, 5, 10, 15, 20, 30, and 50 μM. After gentle shaking and incubation at room temperature for 1 min, the fluorescence intensity of ThT in the solution was measured using a fluorescence spectrophotometer at an excitation wavelength of 443 nm and an emission wavelength of 477 nm. A standard calibration curve was then constructed based on the fluorescence intensity and chebulinic acid concentration. The limit of detection (LOD) was calculated according to the 3σ/slope criterion, where σ represents the standard deviation of blank measurements (n=11), and the slope was obtained from the linear calibration curve.

Selectivity test. To assess the selectivity of the proposed sensing strategy, chebulinic acid or potential interfering substances at a concentration of 5 μM were added to the detection system. The fluorescence responses were then recorded using the proposed aptasensor to evaluate the specificity of the sensing platform.

2.10 Recovery tests in complex sample matrices

Pretreatment of compound blank matrix. A commercial cough syrup was purchased from a local pharmacy and used as the compound blank matrix. Before use, an appropriate amount of the syrup was diluted 50-fold with ultrapure water or selection buffer and vortex-mixed for 1 min. The diluted sample was then centrifuged at high speed for 10 min, and the supernatant was collected and filtered through a 0.22 μm membrane. The resulting filtrate was used as the pretreated compound blank matrix. For the preparation of 10% FBS matrix, fetal bovine serum was diluted with the corresponding buffer.

For recovery experiments, the pretreated sample matrices spiked with different concentrations of chebulinic acid were mixed with the proposed aptasensor, and the fluorescence signals were measured accordingly.

2.11 Statistical analysis

Quantitative data are presented as the mean ± standard deviation (SD). Unless otherwise specified, all measurements were performed in triplicate for each experimental condition. Error bars in the figures represent SD. Data analysis and curve fitting were performed using GraphPad Prism 10.3.0 software.

3. Results and discussion

3.1 Screening of chebulinic acid aptamers by REase-SELEX

The core principle of the REase-SELEX strategy is illustrated in Figure 2A. In this method, the cDNA strand is first hybridized with the DNA library to form a duplex complex. Upon target recognition, aptamer candidates with affinity for chebulinic acid undergo conformational rearrangement, leading to dissociation from the duplex complex. In contrast, non-binding sequences remain in the duplex state. Restriction endonucleases specifically recognize and cleave duplex DNA containing their recognition sites. Therefore, non-binding duplex complexes can be selectively digested, whereas target-binding aptamer candidates are retained for subsequent amplification. Once cleaved, the non-binding duplex products can no longer serve as effective templates for PCR amplification, whereas the target-bound sequences are retained and enriched in

subsequent rounds. This cleavage-based discrimination constitutes the central mechanism of the REase-SELEX method.

In this study, HindIII was selected as the restriction endonuclease, with the recognition site 5′-A↓AGCTT-3′. The screening library was designed with 18-nt forward and reverse primer regions flanking a central region composed of a random sequence and a fixed sequence, which contained the restriction site for enzyme recognition. After removal of the primer regions, the library length was 55 nt, whereas the full-length library was 91 nt. The fixed region was 15 nt in length. The sequence of the fixed region in the library was ATGGAAGCTTGGGAT, and its complementary cDNA sequence was ATCCCAAGCTTCCAT. The forward primer sequence was GGAATCGAGGATTCGTTA, and the reverse primer sequence was ATGTCAGAGTTAGAGGTC (Table S1).

As shown in the schematic illustration (Figure 2B), a total of 12 rounds of selection were carried out, with the selection pressure gradually increased in each round. To improve the matrix adaptability of the selected aptamers for practical sensing applications, specific sample matrices were introduced in later selection rounds. In the eighth round, a compound blank matrix was added to the buffer system, while in the tenth round, 10% FBS was introduced. This strategy was intended to retain aptamer sequences that preserved target recognition capability under realistic analytical conditions. The PCR products from the final round were then subjected to sequencing for identification of enriched candidate aptamers. Representative agarose gel electrophoresis results further verified the PCR amplification, Lambda exonuclease digestion, and ssDNA recovery steps used during the REase-SELEX process (Figure S1).

3.2 Selection and structural characterization of candidate chebulinic acid aptamers

Based on the high-throughput sequencing results, the ten sequences with the highest enrichment levels were initially considered. Among these sequences, the four highest-ranking candidates with GC contents greater than 60% were selected for further evaluation, because their G/C-rich composition was considered favorable for the formation of stable and structurally diverse folded conformations. After removal of the primer-binding regions, the sequences of the four candidate aptamers are listed in Table S1 in descending order of enrichment.

The secondary structure of each candidate aptamer was predicted using the RNAfold web server, and the result is shown in Figure 2C and Figure S2. Most of the predicted structures contained multiple stem-loop motifs, suggesting that these candidate chebulinic acid aptamers could adopt relatively complex folded conformations.

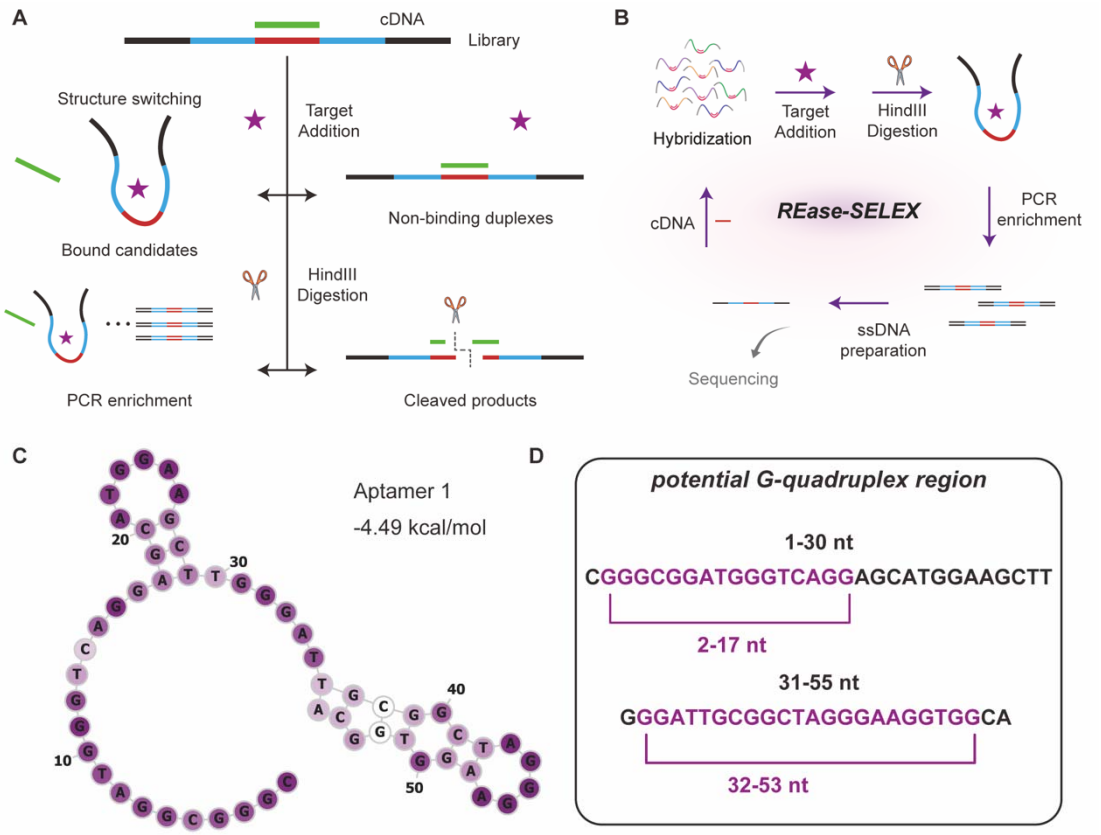

Figure 2. REase-SELEX-based aptamer screening and structural characterization. (A) Separation strategy for binding and non-binding sequences; (B) Schematic illustration of the REase-SELEX screening process; (C) The predicted secondary structure of the Aptamer 1; (D) The potential G-quadruplex-forming regions of the Aptamer 1.

Among the four candidates, Aptamer 1 exhibited the highest enrichment level and the most favorable predicted structural stability, as indicated by its minimum free energy value in the secondary-structure prediction shown in Figure 2C and Figure S2. The thermal stability of the four candidate aptamers was subsequently evaluated. As shown in Figure 3A, Aptamer 1 exhibited the highest Tm in the absence of chebulinic acid, indicating the greatest intrinsic thermal stability among the four candidates. In addition, the Tm of all four aptamers changed after the addition of chebulinic acid, suggesting that chebulinic acid affected the thermal stability or folding behavior of each candidate sequence, consistent with potential aptamer-target interactions.

CD spectroscopy was further used to characterize the folded structures of the candidate aptamers. As shown in Figure 3B and Figure S3, Aptamers 1-4 exhibited a characteristic negative band at approximately 240 nm and a broad positive band in the range of approximately 265-290 nm. These spectral features were generally consistent with the CD characteristics of G-rich nucleic acids capable of forming G-quadruplex-like structures, indicating that all four aptamers could adopt ordered folded conformations in solution. The broad positive bands in the longer-wavelength region, together with the shoulders observed between 270 and 290 nm for some aptamers, suggest that these sequences may not adopt a single G-quadruplex topology. The spectral profiles suggest that the aptamers may adopt heterogeneous G-rich folded conformations, potentially involving G-quadruplex-like structures with mixed topological features. Overall, the CD results support the

propensity of Aptamers 1-4 to form ordered G-rich secondary structures with possible G-quadruplex contributions.

Considering the enrichment level, predicted structural stability, thermal stability, and CD characteristics, Aptamer 1 was ultimately selected for subsequent binding characterization and biosensor development.

Notably, Aptamer 1 contained more than 49% guanine residues, indicating that it is a G-rich sequence with the potential to form higher-order structures such as hairpins and G-quadruplexes. Therefore, the propensity of the aptamer to form G-quadruplex-like structures was further evaluated. QGRS analysis of the 55-nt sequence identified two non-overlapping potential G-quadruplex-forming sequences. When overlapping candidates were also included, a total of 79 potential QGRSs were identified (Table S2), indicating the presence of distinct G-rich segments within the sequence and suggesting a potential for G-quadruplex formation.

As shown in Figure 2D and Table 1, the two representative non-overlapping QGRSs were located at nt 2-17 and nt 32-53, with the sequences GGGCGGATGGGTCAGG and GGATTGCGGCTAGGGAAGGTGG, respectively. Both sequences had a G-score of 20, indicating a relatively high probability of forming G-quadruplex structures. The first candidate region was shorter but contained a dense distribution of G clusters, whereas the second region was longer and harbored multiple consecutive or appropriately spaced guanine residues, both of which are characteristic features of typical QGRSs. These computational predictions were also consistent with the CD spectral characteristics of Aptamer 1, which supported its propensity to form G-quadruplex-like folded structures. Taken together, these results suggest that Aptamer 1 may contain two major potential G-quadruplex-forming core regions, while the numerous overlapping candidates imply the existence of multiple possible folding patterns or conformational alternatives within these G-rich segments. Such structural features may contribute to the secondary structure stability of the aptamer and influence its interaction with chebulinic acid.

Table 1 Non-overlapping QGRS sequences identified in the chebulinic acid aptamer

Position	Length	QGRS	G-Score
2	16	GGGCGGATGGGTCAGG	20
32	22	GGATTGCGGCTAGGGAAGGTGG	20

The underlined nucleotides indicate the potential G-quadruplex-forming core.

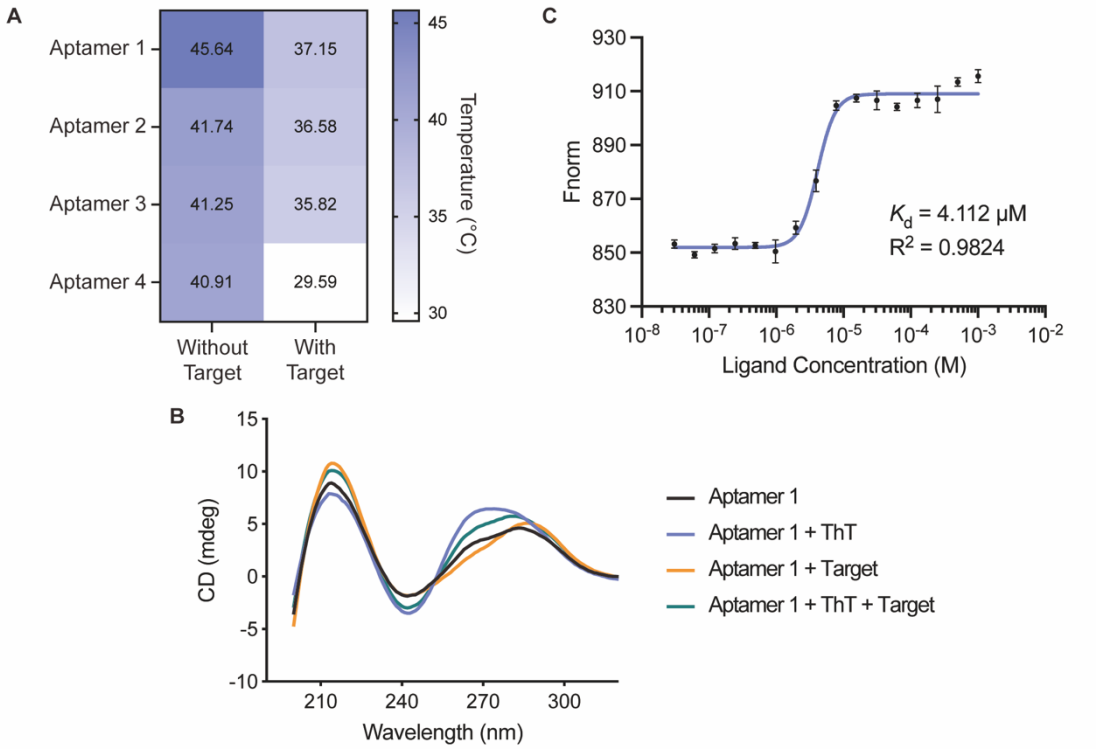

Figure 3. Biophysical characterization of candidate aptamers and binding analysis of Aptamer 1 toward chebulinic acid. (A) Tm of Aptamers 1-4 in the absence and presence of chebulinic acid. (B) CD spectra of Aptamer 1 alone, Aptamer 1 in the presence of ThT, Aptamer 1 in the presence of chebulinic acid, and Aptamer 1 in the presence of both ThT and chebulinic acid. (C) MST analysis of the interaction between Aptamer 1 and chebulinic acid.

3.3 Affinity evaluation of the chebulinic acid aptamer

The binding affinity of the selected chebulinic acid aptamer (Aptamer 1) was evaluated using both MST and a gold nanoparticle (AuNP)-based colorimetric assay. MST was first employed to directly characterize the interaction between Aptamer 1 and chebulinic acid. As shown in Figure 3C, the normalized fluorescence signal changed in a concentration-dependent manner with increasing chebulinic acid concentration. Nonlinear fitting of the MST data yielded an dissociation constant of 4.112 μM, with an R^2 value of 0.9824, suggesting that Aptamer 1 exhibited micromolar-level binding affinity toward chebulinic acid.

The binding performance of the aptamer was further evaluated using a AuNP-based colorimetric assay (Figure 4A). This assay relies on the salt-induced aggregation behavior of citrate-capped AuNPs. Under high-salt conditions, AuNPs tend to aggregate, leading to a color change of the solution from red to blue. Single-stranded nucleic acids can adsorb onto the surface of AuNPs through electrostatic interactions and thereby protect the nanoparticles from salt-induced aggregation, allowing the solution to remain red. Based on this principle, the chebulinic acid aptamer can adsorb onto the AuNP surface and stabilize the AuNPs under saline conditions.

In the presence of chebulinic acid, the aptamer specifically binds to the target and its adsorption on the AuNP surface is reduced. As a result, the AuNPs are insufficiently protected against salt-induced aggregation. This aggregation causes a visible color transition from red to blue. The interaction between the aptamer and chebulinic acid was therefore assessed by measuring the absorbance ratio at 626 nm and 525 nm.

As shown in Figure 4B-C, the AuNP colorimetric assay demonstrated that the selected aptamer exhibited good affinity toward chebulinic acid, as evidenced by the increase in the A626/A525 ratio with increasing chebulinic acid concentration. Furthermore, nonlinear fitting of the AuNP assay data (Figure 4D) yielded an apparent dissociation constant of 2.770 μM, indicating that the selected aptamer possessed favorable binding capability toward the target. Although the Kd values obtained by MST and the AuNP-based assay were not identical, both methods consistently indicated micromolar-level affinity. The difference may be attributed to the distinct detection principles. Taken together, the MST and AuNP results provide complementary evidence supporting the specific binding capability of Aptamer 1 toward chebulinic acid.

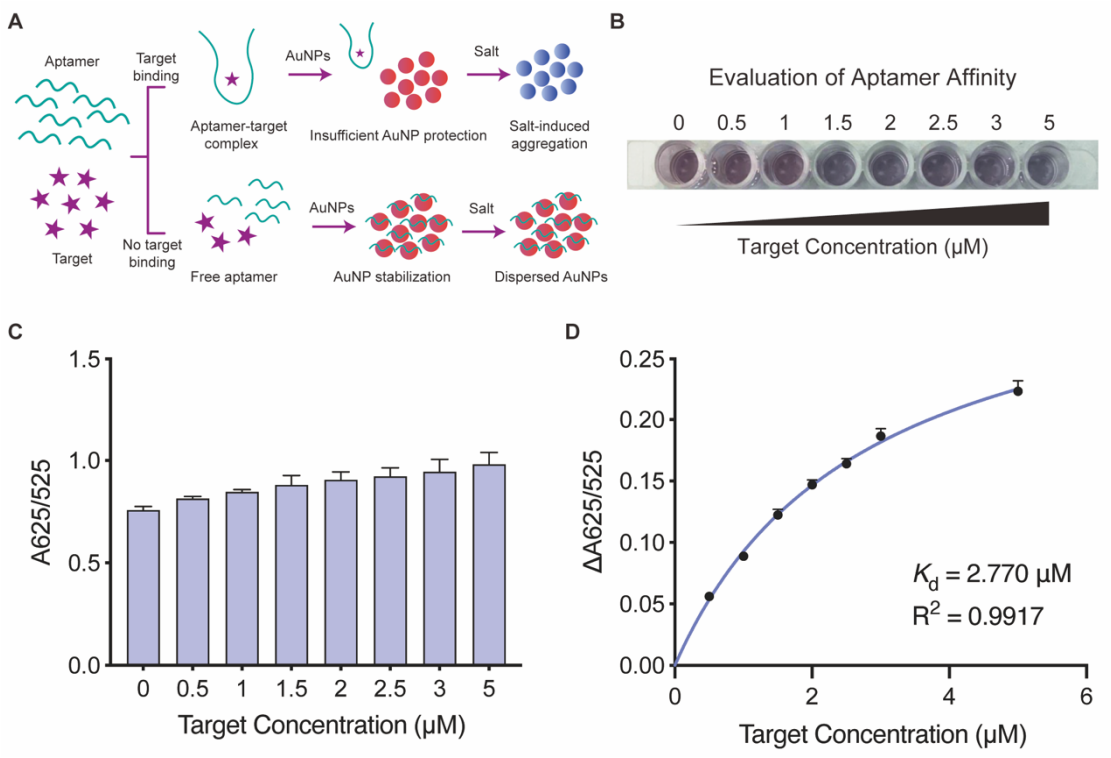

Figure 4. Affinity evaluation of the chebulinic acid aptamer. (A) Schematic illustration of the AuNP-based colorimetric assay for aptamer affinity evaluation; (B) Qualitative results of the AuNP colorimetric assay; (C) Quantitative results of the AuNP colorimetric assay; (D) Determination of the apparent dissociation constant of the chebulinic acid aptamer by the AuNP colorimetric assay.

3.4 Molecular docking analysis of the chebulinic acid aptamer

To obtain preliminary insight into the possible recognition mode between the selected aptamer (Aptamer 1) and chebulinic acid, molecular docking was performed as a computational prediction. Because the 3D aptamer structure was computationally generated, the docking results were used to propose possible aptamer-target interaction modes rather than to provide direct mechanistic evidence.

As shown in Figure 5A, the top 10 docking models suggested several potential binding pockets. Among them, the most probable binding site was located near the 3′-terminal structural region of the aptamer, while another less probable site was identified within a different stem-loop motif. Figure 5B presents the top-ranked predicted three-dimensional docking model. In this model, the predicted binding pocket involved nucleotides G2, G3, C38, G39, A43, A48, and T51. In the corresponding 2D interaction diagram, G39 was predicted to interact with chebulinic acid through a carbon hydrogen bond, whereas G2, G3, C38, A43, and A48 may form

conventional hydrogen bonds with the target (Figure 5C). In addition, several nucleotides within the binding pocket were predicted to contribute auxiliary interactions with chebulinic acid through hydrogen bonding and electrostatic interactions (Figure 5D-E).

Moreover, another docking model suggested an alternative potential binding pocket involving nucleotides G17, G19, C20, A21, A25, A26, G27, and C28 (Figure S4). In this pocket, the aptamer was also predicted to bind chebulinic acid through a combination of hydrogen bonding, electrostatic interactions, and π-π interactions, providing an additional plausible binding mode.

To further compare the potential binding characteristics of the candidate sequences, molecular docking was also performed for Aptamers 2-4. As shown in Figure S5, all three candidate aptamers exhibited predicted interactions with chebulinic acid through multiple noncovalent forces, including hydrogen bonding and π-related interactions. These results suggest that Aptamers 2-4 also possess potential chebulinic acid-binding capability, although Aptamer 1 was selected for subsequent characterization and biosensor development based on its overall enrichment, structural stability, and experimental performance.

Overall, the molecular docking results suggest possible binding modes between the selected aptamer and chebulinic acid. The predicted interactions may involve hydrogen bonding, electrostatic interactions, and π-related interactions. However, these interactions should be regarded as computationally predicted binding modes rather than direct experimental evidence of the recognition mechanism. Further structural and biophysical studies will be needed to experimentally validate the detailed aptamer-target interaction.

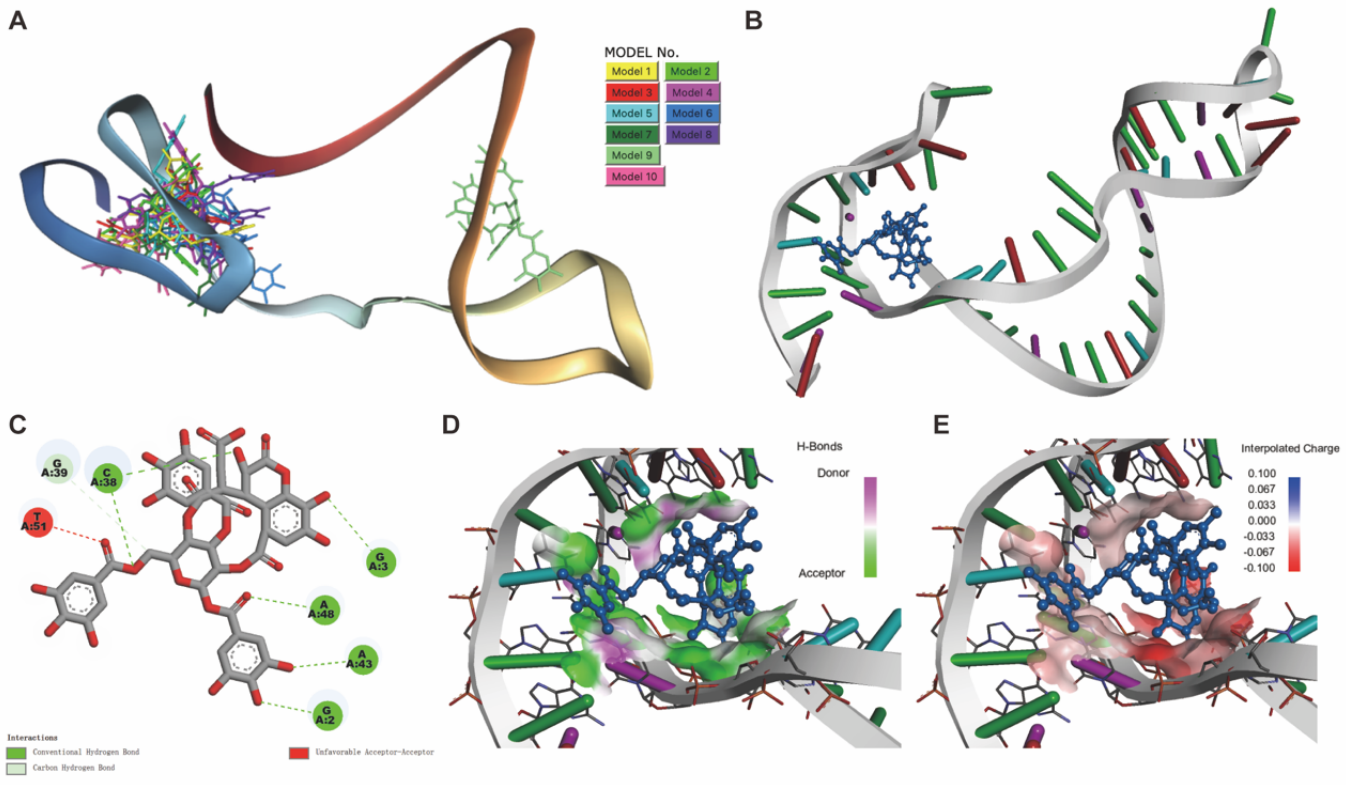

Figure 5. Molecular docking analysis of the chebulinic acid aptamer (major binding pocket). (A) Top 10 molecular docking models; (B) Three-dimensional structure of the aptamer-target complex; (C) Two-dimensional representation of the molecular docking interactions; (D) Hydrogen-bonding interactions and (E) electrostatic interactions between the aptamer and chebulinic acid.

3.5 Feasibility verification and optimization of the label-free aptasensor for chebulinic acid

The feasibility of the proposed label-free aptasensing system for chebulinic acid was first verified. CD spectroscopy was used to evaluate the structural responses of Aptamer 1 under different conditions. As shown in Figure 3B, the addition of either ThT or chebulinic acid caused observable changes in the CD spectrum of Aptamer 1, indicating that both compounds affected the folded conformation of the aptamer. When ThT and chebulinic acid were simultaneously present, the CD spectrum exhibited a distinct response compared with those of Aptamer 1 alone and the corresponding single-component systems. These spectral changes suggest that chebulinic acid can interact with Aptamer 1 and alter the aptamer-ThT-associated folded structure, providing structural support for the feasibility of the sensing mechanism.

As shown in Figure S6, chebulinic acid alone produced only a negligible fluorescence signal, indicating that the target itself caused minimal direct fluorescence interference. In contrast, in the presence of ThT, the fluorescence intensity of the system gradually decreased with increasing chebulinic acid concentration. This observation suggests that binding of chebulinic acid to the aptamer altered the ThT-aptamer interaction, possibly by affecting the folded nucleic acid structures that provide ThT-binding sites, thereby producing a measurable fluorescence response. Taken together, the CD and fluorescence results indicate that chebulinic acid binding induces changes in the aptamer-associated structural environment and consequently modulates the ThT fluorescence signal, suggesting the feasibility of the proposed label-free sensing strategy.

Based on this result, the experimental conditions were further optimized. The order of reagent addition was first investigated. As shown in Figure 6A-C, a more stable fluorescence response was obtained when chebulinic acid and ThT were added simultaneously. Therefore, simultaneous addition of the target and ThT was selected for subsequent experiments. According to the optimization results, the measurement was conducted after incubation for 1 min.

The concentration of ThT was also optimized. As shown in Figure S7, the fluorescence intensity increased with increasing ThT concentration. Considering signal intensity, detection sensitivity, and experimental cost together, 2.5 μM was selected as the optimal final concentration of ThT.

Finally, the pH of the sensing system was optimized. As shown in Figure S8, the sensing platform exhibited relatively stable fluorescence responses over a broad pH range, with the best overall performance observed at pH 7.4. Therefore, pH 7.4 was selected as the optimal pH for subsequent experiments.

Taken together, the optimized operating conditions for the label-free chebulinic acid aptasensor were determined as follows: simultaneous addition of chebulinic acid and ThT, incubation for 1 min prior to measurement, a ThT final concentration of 2.5 μM, and pH 7.4. It should be noted that the 1-min incubation time refers to the fluorescence detection step after sample preparation. After the assay reagents are mixed, the fluorescence signal can be measured immediately following 1 min of incubation. Thus, for prepared standard solutions or pretreated samples, the detection step can be completed within approximately 1-2 min. For complex samples, additional pretreatment steps, including dilution, vortex mixing, centrifugation, and

filtration, are required before measurement, and the total workflow time depends on the sample type and pretreatment procedure.

3.6 Performance evaluation of the label-free chebulinic acid aptasensor

3.6.1 Sensitivity evaluation

To evaluate the sensitivity of the constructed label-free chebulinic acid aptasensor, the effect of different concentrations of chebulinic acid on the ThT fluorescence signal was investigated under the optimized conditions. As shown in Figure 6D, the fluorescence intensity of the system gradually decreased with increasing chebulinic acid concentration, indicating that target binding effectively modulated the interaction between ThT and the aptamer structure and thereby generated a clear fluorescence response. These results demonstrate that the proposed label-free sensing system provides a stable and measurable concentration-dependent response toward chebulinic acid.

A calibration curve was then constructed by plotting the fluorescence intensity against chebulinic acid concentration, as shown in Figure 6E. In the concentration range of 0.1-50 μM, the fluorescence response exhibited a good linear relationship with chebulinic acid concentration, with a regression equation of $Y = -1.260X + 248.6$ and a correlation coefficient of $R^2 = 0.9872$. These results indicate that the proposed aptasensor possesses good quantitative analytical capability and satisfactory linearity within this concentration range. Based on the 3σ/slope criterion, the LOD was calculated to be as low as 8.29 nM, demonstrating the high sensitivity of the sensing platform.

Overall, the developed label-free chebulinic acid aptasensor exhibited a favorable concentration-response relationship, a relatively broad linear detection range, and a low detection limit, highlighting its potential for sensitive detection of chebulinic acid.

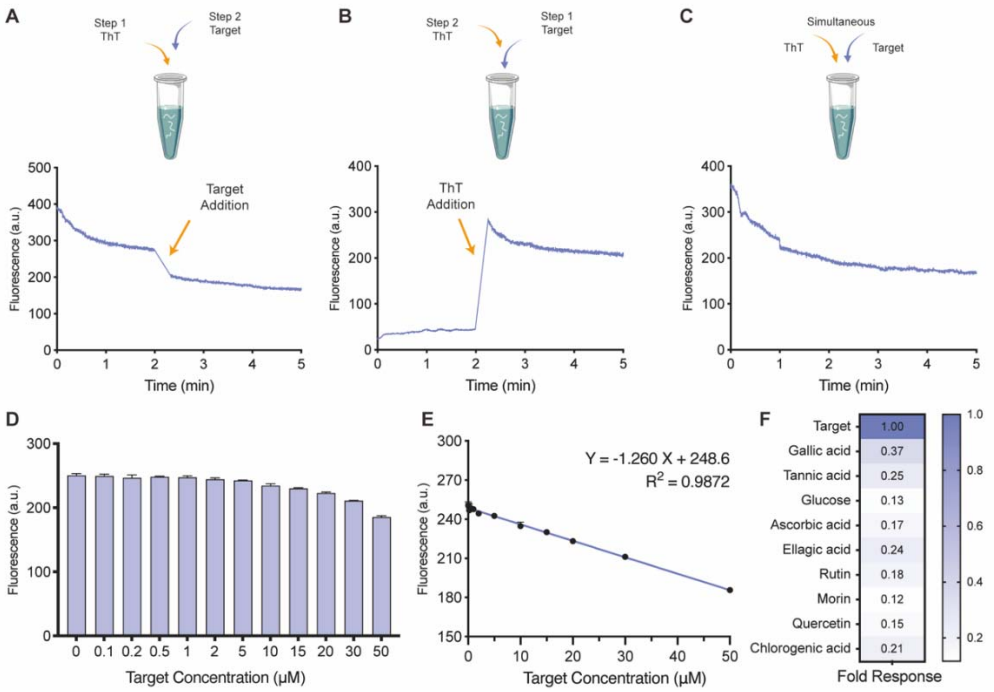

Figure 6. Performance evaluation of the label-free chebulinic acid aptasensor. (A-C) Optimization of reagent addition time; (D) Fluorescence response of ThT at different concentrations of chebulinic acid; (E) Calibration curve for chebulinic acid detection by the aptasensor; (F) Selectivity evaluation of the aptasensor.

3.6.2 Selectivity evaluation

To assess the selectivity of the proposed aptasensor toward chebulinic acid, a range of representative interfering substances was selected, including structurally related polyphenolic compounds, naturally occurring constituents commonly found in plant-derived samples, and common coexisting matrix components. As shown in Figure 6F, chebulinic acid induced the strongest fluorescence response, whereas all interfering substances generated only weak responses that were markedly lower than that of the target.

Although several tested interferents shared structural features with chebulinic acid, the sensor responses toward these compounds remained substantially lower than that toward chebulinic acid. This suggests that the selected aptamer does not simply rely on nonspecific recognition of general polyphenolic scaffolds or hydroxyl-rich structures, but instead exhibits a certain degree of molecular discrimination toward chebulinic acid. In addition, common coexisting matrix components produced only minor fluorescence responses, demonstrating that the aptasensor has good tolerance to potential interference from complex sample constituents.

Taken together, chebulinic acid produced a markedly stronger fluorescence response than all tested interfering substances, confirming the good selectivity of the proposed aptasensor. These results support its potential application for the selective determination of chebulinic acid in herbal formulations, plant extracts, and other complex matrices.

3.7 Recovery evaluation in spiked sample matrices

To evaluate the practical applicability of the proposed aptasensor in complex matrices, recovery experiments were performed using a compound blank matrix and 10% FBS as representative sample models. Chebulinic acid was spiked into these matrices at multiple concentration levels, 0.2, 2, 5 and 10 μM. As shown in Table 2, no target signal was detected in the unspiked samples (ND), indicating that the selected matrices did not produce significant background interference under the present assay conditions.

In both complex matrices, the aptasensor exhibited satisfactory quantitative performance. In the compound blank matrix, the measured values were close to the spiked levels, with recoveries ranging from 97.0% to 102.5% and good repeatability, indicating high accuracy and reliability of the method in this commercially relevant complex background. In comparison, in 10% FBS, the measured values also reflected the spiked concentrations well, with recoveries ranging from 94.3% to 102.9%, demonstrating that the aptasensor retained good applicability in a biological matrix environment. Although the recoveries and precision in FBS showed minor variations compared with those obtained in the compound blank matrix, likely due to matrix effects arising from proteins and other coexisting components in serum, the overall RSD values remained below 6%.

Overall, the proposed aptasensor showed good accuracy and acceptable precision in different complex sample matrices, with recoveries ranging from 94.3% to 102.9% and RSD values all below 6% at all tested concentration levels. These findings indicate that the method has favorable anti-interference capability and promising potential for practical detection of chebulinic acid in complex systems. This performance may also

be attributed to the matrix-adaptive selection strategy employed during aptamer screening, which helped preserve target recognition capability under realistic biosensing conditions. Moreover, the results obtained with the proposed aptasensor showed good agreement with those obtained using the HPLC-based method (Table S3), further supporting the accuracy of the proposed sensing strategy.

Table 2 Recovery tests of chebulinic acid spiked into different sample matrices

Samples	Spiked chebulinic acid (μM)	Measured value (μM)	Recovery (%)	RSD (%)
Compound blank matrix	0	ND	-	-
	0.2	0.194 ± 0.01	97.0	5.15
	2	1.941 ± 0.05	97.1	2.58
	5	5.127 ± 0.11	102.5	2.15
	10	9.861 ± 0.40	98.6	4.06
10% FBS	0	ND	-	-
	0.2	0.189 ± 0.01	94.5	5.29
	2	1.886 ± 0.09	94.3	4.77
	5	4.870 ± 0.09	97.4	1.85
	10	10.291 ± 0.40	102.9	3.89

ND means not detectable.

To further benchmark the analytical performance and practical features of the proposed aptasensor, previously reported chebulinic acid detection methods were summarized and compared in terms of LOD, linear range, sample pretreatment time, detection time, matrix applicability, instrumentation requirements, and relative cost (Table S4). To the best of our knowledge, currently reported methods for chebulinic acid analysis mainly rely on chromatographic, mass spectrometric, electrophoretic, or thin-layer chromatographic platforms, while dedicated colorimetric or electrochemical sensing methods remain limited. Therefore, the present strategy, which integrates an aptamer recognition element with a label-free fluorescent signal readout, provides a distinctive and innovative sensing approach for chebulinic acid detection.

4. Conclusion

In this study, a chebulinic acid-specific DNA aptamer was successfully screened by the REase-SELEX strategy, and its structural characteristics, binding behavior, and sensing performance were systematically investigated. Sequence analysis and structural prediction revealed that the selected aptamer was a G-rich sequence containing multiple stem-loop motifs and potential G-quadruplex-forming regions, suggesting a structurally complex recognition framework. Molecular docking further indicated that the aptamer could recognize chebulinic acid through multiple noncovalent interactions, mainly including hydrogen bonding, electrostatic interactions, and π-related interactions, providing insight into the possible molecular basis of target recognition.

Based on the screened aptamer, a label-free fluorescent aptasensor was developed using ThT as the signal reporter. Under the optimized conditions, the proposed sensing platform exhibited a good linear response toward chebulinic acid over the range of 0.1-50 μM, with a correlation coefficient of 0.9872 and a low LOD of 8.29 nM. In addition, the aptasensor showed satisfactory selectivity against structurally related polyphenols

and common coexisting substances, indicating favorable molecular recognition capability and anti-interference performance.

Furthermore, the practical applicability of the proposed method was validated in a compound blank matrix and 10% FBS, where acceptable recoveries and precision were achieved. These results demonstrate that the aptamer retained effective target recognition ability even in complex sample environments, which may be attributed, at least in part, to the matrix-adaptive screening strategy introduced during the selection process. Overall, this work provides a new aptamer recognition element and a feasible label-free sensing strategy for chebulinic acid detection, and may offer a useful reference for the development of aptamer-based biosensors targeting small-molecule polyphenolic compounds.

Although the signal-off fluorescence response of the current aptasensor may be influenced by nonspecific quenching from complex matrices, the unspiked matrix controls, including the compound blank matrix and 10% FBS, showed only a minor effect on the sensor signal in this study. With further validation in more complex real samples, the proposed label-free aptasensor may serve as a simple, rapid, and low-cost analytical tool for food quality control, functional food evaluation, herbal product standardization, and health-related monitoring.

Acknowledgements

This work was supported by the National Natural Science Foundation of China (21927812), Science and Technology Project of Guozhong Kangjian Group (Project Code: GZKJ-KJXX-QTHT-20230626).

Declaration of Interest Statement

The authors declare that they have no known competing financial interests or personal relationships that could have appeared to influence the work reported in this paper.

References

1. Aashima, Rathi M, Shilpi, et al. Chebulinic Acid: An Incipient Anticancer Agent. *Recent Pat Anticancer Drug Discov*. 2024;19(3):298-307. doi:10.2174/1574892819666230821110429
2. Zhang Q, Ju C, Zhu Q, et al. Preparation and stability of chebulagic acid and chebulinic acid from Terminalia chebula and their biological activity. *Pak J Pharm Sci*. Nov-Dec 2024;37(6):1289-1301.
3. Yeggoni DP, Meti M, Subramanyam R. Chebulinic and chebulagic acid binding with serum proteins: biophysical and molecular docking approach. *J Biomol Struct Dyn*. Jun 2023;41(9):4024-4039. doi:10.1080/07391102.2022.2060862
4. Li R, Liu Y, Li G, et al. Chebulinic acid from Chebulae fructus alleviates influenza virus-induced acute lung injury by inhibiting IDO1-Kyn axis activation. *Phytomedicine*. Nov 25 2025;148:157362. doi:10.1016/j.phymed.2025.157362
5. Munawar TM, Surya Prakash DV, Vangalapati M. Development of response surface methodology for optimization of parameters and quantitative analysis of chebulinic acid from composition of medicinal herbs by HPLC. *Saudi J Biol Sci*. Nov 2019;26(7):1809-1814. doi:10.1016/j.sjbs.2018.02.013
6. Chen K, Zhu L, Du Z, et al. Docking-aided rational tailoring of a fluorescence- and affinity-enhancing aptamer for a label-free ratiometric malachite green point-of-care aptasensor. *J Hazard Mater*. Apr 5 2023;447:130798. doi:10.1016/j.jhazmat.2023.130798
7. Chen K, Li X, Dong K, et al. SMART strategy-driven engineering of multifunctional aptamers: Multifaceted applications in biosensing, toxicity masking, and sustained-release antibacterial. *J Hazard Mater*. Feb 1 2026;503:141159. doi:10.1016/j.jhazmat.2026.141159

8. Jahnke K, Grubmüller H, Igaev M, Göpfrich K. Choice of fluorophore affects dynamic DNA nanostructures. *Nucleic Acids Res*. Apr 19 2021;49(7):4186-4195. doi:10.1093/nar/gkab201
9. Chen K, Zhu L, Li J, et al. High-content tailoring strategy to improve the multifunctionality of functional nucleic acids. *Biosens Bioelectron*. Oct 1 2024;261:116494. doi:10.1016/j.bios.2024.116494
10. Chen X, Chen K, Du Z, et al. Fusion of binary split allosteric aptasensor for the ultra-sensitive and super-rapid detection of malachite green. *J Hazard Mater*. Mar 5 2022;425:127976. doi:10.1016/j.jhazmat.2021.127976
11. Gruber AR, Lorenz R, Bernhart SH, Neuböck R, Hofacker IL. The Vienna RNA websuite. *Nucleic Acids Res*. Jul 1 2008;36(Web Server issue):W70-4. doi:10.1093/nar/gkn188
12. Antczak M, Popenda M, Zok T, et al. New functionality of RNAComposer: an application to shape the axis of miR160 precursor structure. *Acta biochimica Polonica*. 2016;63(4):737-744. doi:10.18388/abp.2016_1329
13. Yan Y, Zhang D, Zhou P, Li B, Huang S-Y. HDOCK: a web server for protein–protein and protein–DNA/RNA docking based on a hybrid strategy. *Nucleic Acids Research*. 2017;45(W1):W365-W373. doi:10.1093/nar/gkx407
14. Grabar KC, Freeman RG, Hommer MB, Natan MJ. Preparation and Characterization of Au Colloid Monolayers. *Anal Chem*. 1995/02/15 1995;67(4):735-743. doi:10.1021/ac00100a008
15. Turkevich J, Stevenson PC, Hillier J. A study of the nucleation and growth processes in the synthesis of colloidal gold. 10.1039/DF9511100055. *Discussions of the Faraday Society*. 1951;11(0):55-75. doi:10.1039/DF9511100055
16. Zhu L, Miao M, Shao X, et al. A Universal Electrochemical Biosensor Using Nick-HCR Nanostructure as Molecular Gate of Nanochannel for Detecting Chromium(III) Ions and MicroRNA. *Anal Chem*. 2019;91(23):14992-14999. doi:10.1021/acs.analchem.9b03489
17. Zhu L, Li S, Shao X, et al. Colorimetric detection and typing of E. coli lipopolysaccharides based on a dual aptamer-functionalized gold nanoparticle probe. *Microchimica Acta*. 2019/01/14 2019;186(2):111. doi:10.1007/s00604-018-3212-9